Chemistry–A European Journal
Research Article
doi.org/10.1002/chem.202404572
Chemistry Europe
European Chemical Societies Publishing
www.chemeurj.org

Label-Free 3D Cell Imaging Using Hydrogels Functionalized with Switchable Iridium Complexes

Federica Fiorini+,[a, f] Elena Longhi+,[a, g] Ariadna Lazaro+,[b] Daria Di Prisco,[c, d] Giulia Tamboia,[c, d, e] Giuseppe Alonci,[a] Luigi Menduti,*[d] and Luisa De Cola*[b, c, d]

The use of fluorescent labels is the most common tool to visualize cells. However, the internalization of dye molecules often modifies the cell behavior. In this paper we demonstrate that it is possible to transiently label cells using a 3D scaffold, a hydrogel, covalently functionalized with luminescent cyclometalated iridium(III) complexes. The unique feature of our design is that the complexes are emissive only when they interact with the cell membrane while their emission is quenched in water. We exploited this feature to perform real-time and staining-free cell visualization and imaging. Iridium functionalized hydrogels are very weakly luminescent when immerged in culture media. When cells are added to them, they interact with the iridium complexes, covalently linked to the gel, and their lipophilic membrane "switches on" the luminescence enabling a clear and dynamic, real-time 3D visualization of cell proliferation. A complete photophysical and biological study of the materials is presented which demonstrates the potential of our methodology for 3D-realtime cell tracking.

Introduction

Hydrogels are three-dimensional (3D) networks composed of cross-linked hydrophilic polymers, able to swell in water without dissolution.[1,2] Due to their ability to absorb large volumes of water,[3] and their porous structure, hydrogels represent valuable platforms for the diffusion of oxygen, nutrients and growth factors. These properties combined with the possibility of engineering mechanical properties and bio-functionalities *via* modification of the polymeric network, make hydrogels particularly appealing for applications in drug delivery,[4,5] tissue regeneration,[6,7] sensing and imaging.[8,9]

In particular, hydrogels have been successfully employed as 3D-matrices to support cell growth.[10] 3D scaffolds are of great interests in biology, due to their ability to mimic natural tissues, to allow organoids growth since enables cells proliferation and organization.[11,12]

Study of living cells and real-time biological processes in such matrices, relies on fluorescence microscopy through the use of imaging agents.[13] The commonly employed labels are organic fluorescent dyes[14] with high photoluminescence quantum yields. As drawbacks, such chromophores suffer of photobleaching over time, short excited state lifetimes preventing the use of time-gated techniques, and small Stokes shift which may lead to overlap of excitation/emission light.[15] Overall, organic chromophores still do not meet optimal requirements for cellular applications and thus, the development of new imaging probes is still a relevant research topic.

In this context, transition-metal complexes represent very appealing dyes for cell visualization.[16] They have outstanding photophysical properties, such as (1) high luminescence quantum yield, (2) hundreds of nanoseconds to microseconds lifetimes,[17] (3) enhanced photostability[18] and (4) large Stokes shift.[19] Furthermore, metal complexes allow for ease-tuning of the photophysical properties by ligand modification.[20] Due to the triplet nature of their excited state, they behave as dioxygen sensors since their emission properties depend on the oxygen concentration in the surrounding environment.[21] Unfortunately, they often show high cytotoxicity and therefore their implementation in biology is still limited. In fact, the use of a label that must be internalized by the cells, is a questionable method since the presence of the non-natural molecules can dramatically modify the cell behavior.

Recently, several reports on luminescent self-emissive hydrogels and hybrid hydrogels incorporating emitters in their

[a] Dr. F. Fiorini,+ Dr. E. Longhi,+ Dr. G. Alonci
Institut de Science et d'Ingénierie Supramoléculaires (I.S.I.S.), Université de Strasbourg, 8 allée Gas-pard Monge, Strasbourg 67000, France
[b] Dr. A. Lazaro,+ Prof. L. De Cola
Institut für Funktionelle Grenzflächen (IFG), Karlsruhe Institute of Technology (KIT), Eggenstein-Leopoldshafen 76344, Germany
E-mail: luisa.decola@unimi.it
[c] D. Di Prisco, G. Tamboia, Prof. L. De Cola
Department of Biochemistry, Istituto di Ricerche Farmacologiche Mario Negri IRCCS, Milan 20156, Italy
[d] D. Di Prisco, G. Tamboia, Dr. L. Menduti, Prof. L. De Cola
Department of Pharmaceutical Science, Università degli Studi di Milano, Milan 20133, Italy
E-mail: luigi.menduti@unimi.it
[e] G. Tamboia
Department of Chemistry, Biology and Biotechnology, Università degli Studi di Perugia 06123, Italy
[f] Dr. F. Fiorini+
current address: Department of Drug Metabolism & Pharmacokinetics, Boehringer Ingelheim Pharma GmbH & Co. KG, Biberach, Germany
[g] Dr. E. Longhi+
current address: Broad Institute of MIT and Harvard, Cambridge, MA, USA
[+] These authors contributed equally to this work.

Supporting information for this article is available on the WWW under https://doi.org/10.1002/chem.202404572

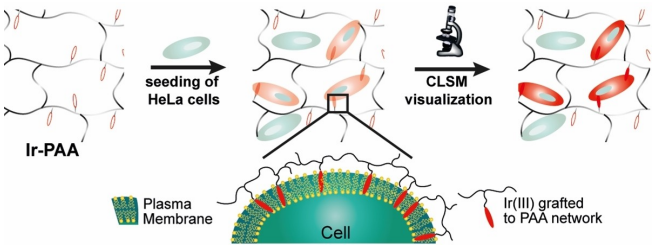

Figure 1. Schematic representation of the "switch-off/on" mechanism of the Ir-hydrogels emission.

matrices have been published.[22,23] However, to the best of our knowledge, no dynamic imaging platform allowing for motion and visualization of cells in real-time has been reported.

In this work, we demonstrate that it is not necessary to label the cells in a permanent way, but it is possible to turn on the emission of luminescent molecules covalently bound to a biocompatible hydrogel, only when the cells get in contact with the 3D matrix. This dynamic imaging strategy combines the advantages of the 3D matrix, the hydrogel, with those of luminescent metal complexes, and in particular with the switch on/off of them depending on the surrounding environment. Interaction of the cells with the hydrophobic ligands of the complex allows for internalization of the complex in the (hydrophobic) membrane. Limited oxygen diffusion and rigidity of the environment, preserves suitable triplet state population, thus allowing switch-on of the phosphorescent dye emission. The concept is depicted in Figure 1 and it is demonstrated with the new iridium complexes synthesized and characterized, their photophysical properties and the cell experiments.

Results and Discussion

As 3D scaffolds, we selected polyamidoamines (PAA) synthetic hydrogels because their low cytotoxicity,[24] easy preparation at room temperature *via* Michael-type polyaddition of primary amines to *N,N'*-methylene(bisacrylamide), followed by the addition of a diamine crosslinker.[25]

In addition their rheological properties can be easily tuned by introducing substituents and using different crosslinkers. As for the metal complexes, iridium complexes were the dyes of choice due to their outstanding photophysical performance and due to their facile functionalization enabling conjugation to the hydrogel network. We selected hydrophobic highly conjugated cyclometalated ligands to shift the absorption in the visible region, and favor interactions with apolar environments and as ancillary ligand a substituted bipyridine to introduce a charge and favor water solubility. The synthesis of Ir-PAAs was performed, as for the unsubstituted gels, *via* Michael-addition reaction.

Synthesis and Characterization of Ir(III) Probes

We designed and synthesized two red emitting Ir(III) complexes containing the hydrophobic cyclometalating ligands, 6-(phenyl)phenanthridine, and as ancillary ligand 2,2'-bipyridine opportunely functionalized with an amino linker to allow a co-polymerization reaction; **Ir1** (Figure 2a) bears all-carbon amine linker while, **Ir2** is functionalized with a PEG-amino linker (Figure 2b) to enhance solubility in aqueous media. The compounds were synthesized following procedures described in the literature (see SI).[26,27]

The photophysical properties of both complexes were investigated in different solvents. The UV-vis absorption spectra (Figure 2) of the complexes in water and dichloromethane (DCM) at room temperature show in the UV region (250–400 nm) intense bands with molar extinction coefficients (ε) of the order of $10^4\ M^{-1}cm^{-1}$ assigned to π-π^* transitions localized on the cyclometalated and bipyridine ligands. The bands at lower energies (420 nm) are assigned to spin-allowed and spin-forbidden singlet and triplet metal-to-ligand charge transfer (MLCT) transitions. They involve the iridium unit and the pyridine moieties of both the (phenyl)phenanthridines and bipyridine ligands, as described for analogous complexes.[28,29]

The emission profiles of the **Ir1** and **Ir2** complexes and their photophysical data in air-equilibrated and degassed water and DCM solutions are reported in Figure 2 and Table 1.

In bis-cyclometalated Ir(III) complexes as $[Ir(C\ N)_2(N\ N)]^+$, the room-temperature phosphorescence is mainly dictated by the $Ir(C\ N)_2$ fragment when the singlet and triplet energies of the ancillary ligand are significantly higher than those of the C N ligand.[30,31] Even though the bipyridine is a good electron acceptor group, the π-extended scaffold of the phenanthridine moietes allows for a lower energy transition which can be assigned to ^{3}MLCT. The compounds display a bright red emission (λ_{em} = 625 nm) in deareated DCM, slightly red-shifted in water (λ_{em} = 635 nm). Such positive solvatochromism points towards a stronger stabilization of the excited state in polar solvents as expected for the metal-to-ligand charge transfer nature of the luminescent state.

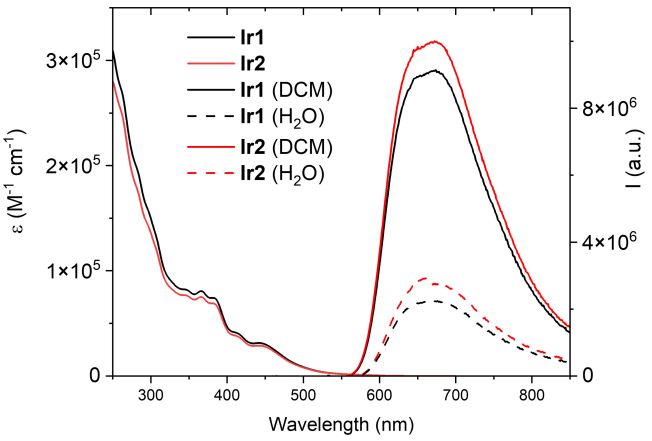

Figure 2. Absorption spectra of **Ir1** (black) and **Ir2** (red) in DCM and emission spectra in degassed DCM (solid lines) and water (dashed line) solutions. λ_{exc} = 405 nm.

Table 1. Photophysical data of the **Ir1**, **Ir2** complexes and **Ir1-PAA**, **Ir2-PAA** hydrogels. λ_{exc} = 405 nm.

	Solution	*DCM*		*water*	
		Air-equilibrated	*degassed*	*Air-equilibrated*	*degassed*
Ir1	λ_{em} [nm]	625	625	635	635
	PLQY [%]	7	24	4	7
	$\tau^{[a]}$ [μs]	0.76	2.01	0.23(31.7 %) 0.8(68.3 %)	0.43(14.1 %) 1.95(85.9 %)
Ir2	λ_{em} [nm]	625	625	635	635
	PLQY [%]	10	28	7	11
	$\tau^{[a]}$ [μs]	0.71	2.34	0.33(27.8 %) 0.69 (72.2 %)	0.59 (10.4 %) 1.45 (89.6 %)
	Hydrogel	*Dry*		*DMEM*	
Ir1-PAA	λ_{em} [nm]	510, 650		510, 650	
	PLQY [%]	14		7	
	$\tau^{[a]}$ [μs]	2.01		1.12	
Ir2-PAA	λ_{em} [nm]	510, 650		510, 650	
	PLQY [%]	17		9	
	$\tau^{[a]}$ [μs]	1.94		0.95	

[a] Recorded at λ_{em} = 650 nm.

Both complexes show mono-exponential excited state lifetimes both in degassed and air-equilibrated DCM with values significantly affected by the presence of molecular oxygen in solution. In water, the complexes display a biexponential luminescent lifetime (Table 1). The biexponential decay is attributed to the partial aggregation of the complexes, caused by their hydrophobic large, conjugated ligands that lower the solubility of the complex in water and quench the emission. Emission quantum yields (PLQY) of the compound are much higher in DCM than in water and, as expected, drop dramatically in air-equilibrated samples due to the triplet nature of the emissive state (Table 1).

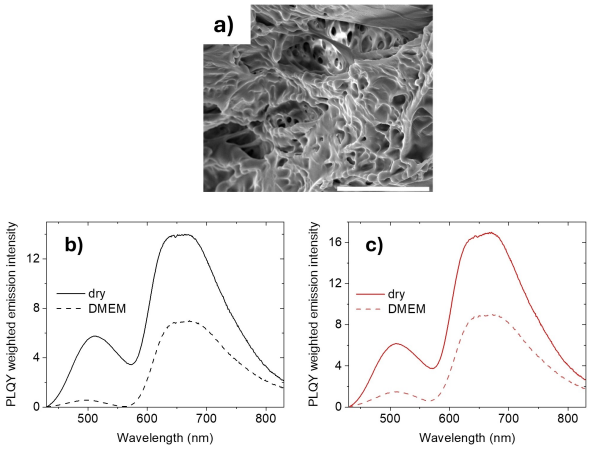

Figure 3. a) SEM image of the morphology of **Ir1-PAA**, scale bar is 100 μm; b) emission spectra of **Ir1-PAA** in dry state (solid line) and equilibrated in DMEM (dashed line); c) emission spectra of **Ir2-PAA** in dry state (solid line) and equilibrated in DMEM (dashed line). λ_{exc} = 405 nm.

Synthesis and Characterization of Ir-PAAs Hydrogels

The Ir complexes were grafted *via* co-polymerization reaction to the backbone of a PAA hydrogel scaffold. The obtained materials were named **Ir1-PAA** and **Ir2-PAA** (Figure S2A).

The hydrogels were synthesized by Michael-type polyaddition of γ-aminobutyric acid (GABA) to methylenebisacrylamide (MBA) and crosslinked with pentaethylenehexamine (PEHA). The iridium complexes **Ir1** and **Ir2**, equipped with an amino terminal group (Figure 2), were introduced into the polymeric structure *via* Michael addition to MBA (≃0.05 nmol/mol Ir-complex/MBA).

Ir1-PAA morphology was assessed by scanning electron microscopy (SEM; Figure 3a), which revealed high porosity (pores diameter range = 20–80 μm). **Ir1-PAA** showed that the equilibrium swelling of the hydrogel was reached after being immersed in water overnight. The swelling ratio (SR) was found to be SR = 424 % for **Ir1-PAA** and SR = 430 % for **Ir2-PAA** and remained constant for the four-days-study period. We assumed **Ir2-PAA** to have similar porous structure properties, since it has the same polymeric network, similar SR and it was synthesized with the same protocol except for the use of **Ir2** instead of **Ir1**.

The hydrogels were dark yellow in dry state and pale yellow-transparent in the swelling-state, after equilibration in deionized water (Figure S2B). Interestingly, when excited at 365 nm with an UV lamp, both **Ir1** and **Ir2** showed bright red emission only in the dry state, as effect of the emission switch of the embedded Ir-complex in response to different environments (Figure S4).

The photoluminescence (PL) behavior of the iridium gels was studied in dry and swelling-state in Dulbecco's Modified Eagle Medium (DMEM). The gels have, as expected, the same

switching behavior, being more emissive in the dry state, see emission of **Ir1-PAA** and **Ir2-PAA** in Figure 3b, c.

In both conditions, **Ir1-PAA/Ir2-PAA** show two main bands, the first with maxima around 510 nm, was attributed to the emission of the PAA network composing the hydrogel. PAA-based materials are known to have fluorescence emission under UV irradiation presumably originating from lone pair electrons on the tertiary nitrogen present in the structure. The second band at lower energy was perfectly overlapping with the emission spectrum of **Ir1** and **Ir2**, therefore confirming the ^{3}MLCT character of the emission. The photophysical parameters obtained are summarized in Table 1.

Ir1-PAA/**Ir2-PAA** emission excited states were monitored at 650 nm and exhibited excited state lifetimes in dry condition (2.01 μs for **Ir1-PAA**; 1.94 μs for **Ir2-PAA**), and in DMEM equilibrated samples (1.12 μs for **Ir1-PAA**; 0.95 μs for **Ir2-PAA**). The same trend of higher emission intensity was observed when measuring PLQY (Table 1). Considerable quenching of the luminescence in DMEM equilibrated samples could be attributed to both the dissolved oxygen quenching (responsible for lower emission in the swollen state) and to the polarity of the environment that could promote aggregation of the complexes.

Cell Studies

The iridium containing hydrogels, **Ir1-PAA** and **Ir2-PAA**, were examined for their ability to support 3D cell proliferation.[32] Previous research demonstrated excellent *in vitro* and *in vivo* biocompatibility of PAA-based hydrogels.[33]

The potential of Ir-PAAs scaffolds, incorporating an imaging Ir dye, was assessed for real-time, 3D live-cell imaging applications. Initially, the behavior of the acellular **Ir1-PAA** in both its dry state and, when equilibrated with Dulbecco's modified eagle medium (DMEM), was analyzed using CLSM. In the acellular DMEM-swollen sample, emission from the **Ir1** complex was not observed (Figure S8). Interestingly, upon seeding HeLa cells a red emission, centered at 640 nm, was detected throughout the cell's plasma membrane (Figure 4a). The hypothesis is that the emission enhancement is due to the good dispersibility of the Ir complex within the lipophilic layer, preventing aggregation and rigidifying the complex. Additionally, oxygen diffusion, being hindered in the cell membrane might play a significant role.

Indeed, it is known that the oxygen permeability coefficient of the plasma membrane is twice as low as that of a water layer of the same thickness,[34] therefore the transition of the Ir-probe from the extracellular aqueous matrix into the membrane allowed for shielding the complex excited state from the dioxygen dissolved in the extracellular environment. All these factors enabled the compound to switch on its bright red luminescent emission. A similar phenomenon has been observed in luminophore-labeled protein systems.[35]

This made possible to detect HeLa cells within and across the hydrogel without any cell labeling or nuclear staining. The red emission was activated only when the cells interacted with

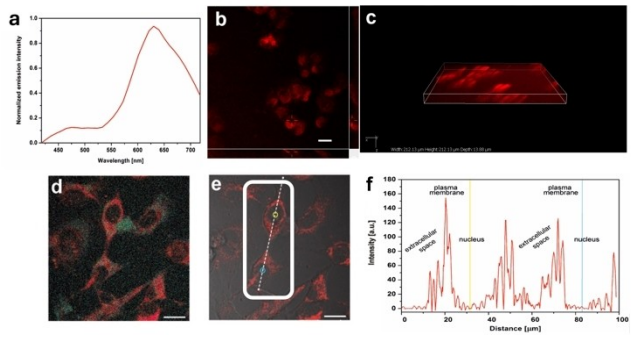

Figure 4. a) CLSM emission spectrum from the plasma membrane of cells grown onto **Ir1-PAA**; b) Z-stack and c) 3D images of HeLa cells onto **Ir1-PAA**; d) true color living HeLa cells on **Ir1-PAA**; e) channels overlay; f) luminescence intensity profile across the line shown in the white box, corresponding to extracellular region, membrane and nuclear region of two cells. Scale bar is 20 μm and CLSM 60x magnification. λ_{em} = 560–750 nm.

the complex in a transient way. The localization of the red luminescence from the cell plasma membrane was also visualized by CLSM Z-stack images at increasing depths along the Z-axis and in 3D for both the **Ir1-PAA** and **Ir2-PAA** (Figure 4b,c and Figure 5a,b respectively). The luminescence intensity profile of HeLa cells growing on the **Ir-PAA** scaffolds revealed a high signal ratio exclusively from the lipophilic membrane, while no signal was detected from other regions such as the cytoplasm, nuclei, or extracellular region. The linker connecting the Ir complexes to the hydrogel network prevents the full penetration of dyes into the cytosol. The nature of Ir complexes, bearing highly hydrophobic aromatic ligands, in combination with the positive charge of the complex, facilitates this interaction.[36,37]

Additionally, it was confirmed that **Ir1** and **Ir2** were not localized in nuclei, by performing staining of the nucleus with

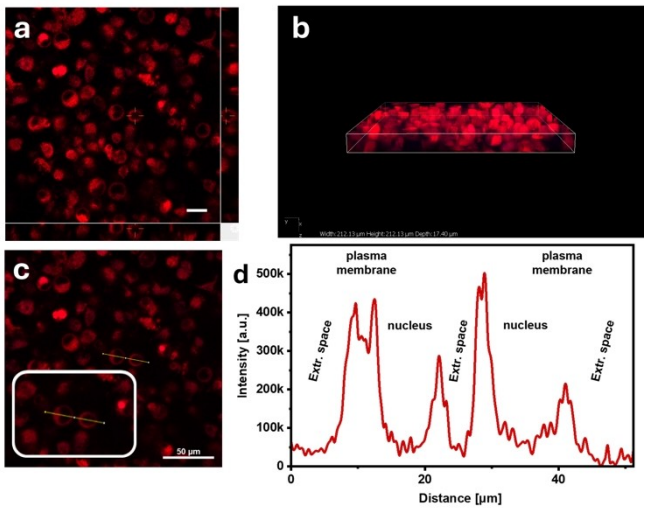

Figure 5. CLSM of cells grown onto **Ir2-PAA**: a) Z-stack, scale bar is 20 μm, b) 3D image, c) true color living HeLa cells; d) luminescence intensity profile across the line in the white box, corresponding to extracellular region, membrane and nuclear region of two cells. CLSM 60x magnification. λ_{em} = 560–750 nm.

Hoechst 33342. Figure 6 shows a comparison of stained and unstained cells for the two different Ir complexes **Ir1** and **Ir2**.

Citotoxicity Studies

To evaluate the cyto-compatibility of Ir-PAA, the viability of HeLa cells seeded onto the scaffolds was monitored over 96 hours. The results indicated that Ir-PAA gels provide a suitable 3D platform for cell growth and that the covalently bound Ir complexes do not negatively impact cell proliferation (Figure S6).

Since **Ir1**/**Ir2** only differ in the PEG/non-PEG linker endocytosis processes and the lipophilic-driven interaction with the plasma membrane were studied for **Ir1-PAA** which we selected as model. HeLa cells were cultured on the **Ir1-PAA** at 4 °C for 1 hour (Figure 7).

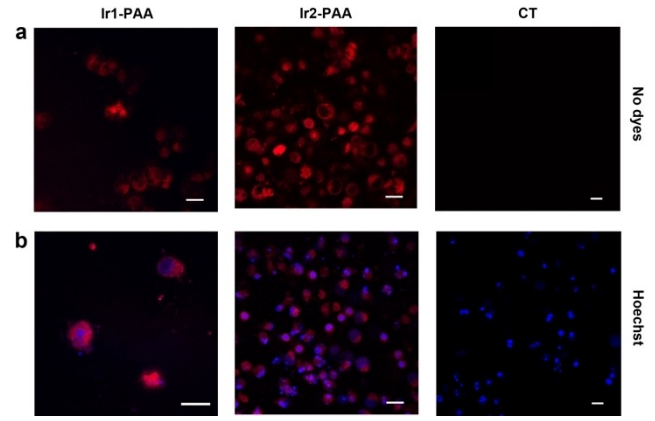

Figure 6. CLSM images of **Ir1-PAA**, **Ir2-PAA** and **control** (**CT**; unfunctionalized PAA): a) without Hoechst 33342, b) after the addition of Hoechst 33342. Scale bar is 20 μm.

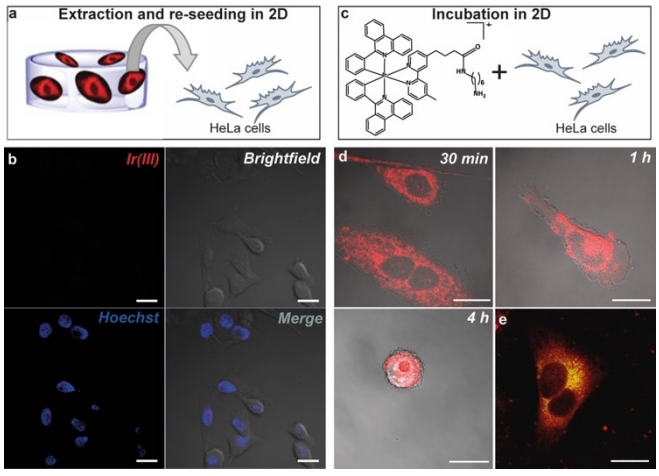

Figure 7. a) Extraction of HeLa cells from the **Ir1-PAA** by trypsinization and re-seeding on petri dishes; b) visualization of HeLa extracted from the hydrogel, clearly showing no residues of **Ir1** complex; c) 2D incubation of free **Ir1** complex with HeLa cells; d) uptake of **Ir1** complex at a concentration 15 nM, after 30 min, 1 h and 4 h of incubation; e) colocalization of the uptaken **Ir1** complex and the green ER-Tracker visualized in yellow; f) Scale bar is 20 μm and magnification is 60×.

After the treatment, a bright red emission was still visible from the cell's membrane, confirming the absence of endocytic processes. We also demonstrated that there were no leakage phenomena of the iridium complexes into the cells. HeLa cells, cultured for seven days on the **Ir1-PAA** scaffold, were removed from the scaffold by trypsin treatment, seeded in 2D glass-bottom petri dishes, and imaged (Figure 7a, b, Figure S7). CLSM visualization of live cells clearly showed no traces of **Ir1** complex (Figure 7b, Figure S7).

Currently, only a few fluorescent membrane dyes are available for membrane staining purposes.[38,39] However, they suffer from rapid internalization, diffusion throughout the entire cell,[40] fast detachment from the plasma membrane,[41] and they allow only a short-time imaging window.[35] With our system, we were able to visualize and image the cell membrane of HeLa proliferating into the **Ir1-PAA** scaffold for up to seven days.

To test the stability of the covalent binding of **Ir1** to the gel, we analyzed the cytotoxicity and internalization mechanism of the free **Ir1** complex. HeLa cells were cultured in 2D and incubated with the Ir-complex (Figure 7c, d). After 30 min of incubation, cells were imaged, and an intense red luminescence was detected in the cytoplasm region upon excitation at 405 nm. After 1 hour of incubation, many cells exhibited a clear uptake of **Ir1**, also diffusing into the nuclear region, which was never observed in the 3D **Ir1-PAA** investigation. Interestingly, the cells began to show signs of shrinkage, membrane blebbing, and plasma membrane vesiculation, indicating an unhealthy (apoptotic) state.[42,43] This behavior became more evident with a four-hour incubation (Figure 7d). Colocalization studies were performed by adding ER-Tracker dye, which evidenced the uptake of **Ir1** complex also in the endoplasmic reticulum (ER), Figure 7e. We hypothesized that the accumulation of the **Ir1** in the ER regions might have induced ER stress and calcium release into the cytoplasm, triggering the onset of apoptotic cell death mechanisms.[37] The cells were also incubated with the iridium probe at 4 °C for 1 hour, showing as expected no internalization (Figure S9), since for the free complex the uptake and the subsequent localization are due to endocytosis processes.

These results imply that when the **Ir1** complex is not covalently linked to the polymeric network, it is fully internalized into the cells, localizes in all cell compartments, and causes apoptosis of the HeLa cells, as reported in other studies.[44,45]

The covalent grafting to the hydrogel does not allow full internalization of the complex, thereby preventing any toxicity.

Conclusions

In conclusion, we have successfully designed and synthetized two novel phosphorescent environment-sensitive 3D hydrogel scaffolds (**Ir1-PAA**) for staining-free real-time *in vitro* imaging of cells. These new materials displayed high cyto-compatibility and enabled clear imaging of the cells up to seven days, without additional cell staining and enabling the dynamic behavior of the cells. Such finding provides a new tool useful for cell-imaging as an alternative to the use of external dyes

that may hamper the cells. We have attributed the "off/on" switching of the luminescence to the hydrophobic interaction between the **Ir1**/**Ir2** complexes and the cell membrane, which shields the triplet excited state of the complex from the dioxygen-quenching and avoiding aggregation while enhancing the rigidity of the system, resulting in a bright red emission. To the best of our knowledge, the **Ir1-PAA**/**Ir2-PAA** scaffolds presented here are the first 3D platforms with an embedded "off/on" phosphorescent dye.

Supporting Information

The authors have cited additional references within the Supporting Information (Ref. [27, 46–52]).

Acknowledgements

L.M and L.D.C. gratefully acknowledge PRIN 2020 AStraLI 2020CBEYHC. The authors gratefully acknowledge the Mass Spectrometry facility of the Unitech COSPECT at the University of Milan (Italy) to perform the mass spectrometry analyses. Open Access publishing facilitated by Università degli Studi di Milano, as part of the Wiley - CRUI-CARE agreement.

Conflict of Interests

The authors declare no conflict of interest.

Data Availability Statement

The data that support the findings of this study are available from the corresponding author upon reasonable request.

Keywords: 3D hydrogels · iridium complex · "off-on" luminescence · staining-less · real-time cells visualization

[1] T. C. Ho, C. C. Chang, H. P. Chan, T. W. Chung, C. W. Shu, K. P. Chuang, T. H. Duh, M. H. Yang, Y. C. Tyan, *Molecules* **2022**, *27*, 2902.
[2] S. Bashir, M. Hina, J. Iqbal, A. H. Rajpar, M. A. Mujtaba, N. A. Alghamdi, S. Wageh, K. Ramesh, S. Ramesh, *Polymer* **2020**, *12*, 1–60.
[3] Z. Ahmad, S. Salman, S. A. Khan, A. Amin, Z. U. Rahman, Y. O. Al-Ghamdi, K. Akhtar, E. M. Bakhsh, S. B. Khan, *Gels* **2022**, *8*, 167.
[4] Y. Cheng, H. Zhang, H. Wei, C. Y. Yu, *Biomater. Sci.* **2024**, *12*, 1151–1170.
[5] M. Vigata, C. Meinert, D. W. Hutmacher, N. Bock, *Pharmaceutica* **2020**, *12*, 1–45.
[6] S. Mantha, S. Pillai, P. Khayambashi, A. Upadhyay, Y. Zhang, O. Tao, H. M. Pham, S. D. Tran, *Materials* **2019**, *12*, 3323.
[7] P. Bertsch, M. Diba, D. J. Mooney, S. C. G. Leeuwenburgh, *Chem. Rev.* **2023**, *123*, 834–873.
[8] A. Herrmann, R. Haag, U. Schedler, *Adv. Healthcare Mater.* **2021**, *10*, 202100062.
[9] a) F. Pinelli, L. Magagnin, F. Rossi, *Mater. Today Chem.* **2020**, *17*, 100317; b) M. A. Mohamed, A. Fallahi, A. M. A. El-Sokkary, S. Salehi, M. A. Akl, A. Jafari, A. Tamayol, H. Fenniri, A. Khademhosseini, S. T. Andreadis, C. Cheng, *Prog. Polym. Sci.* **2019**, *98*, 101147.
[10] J. Lou, D. J. Mooney, *Nat. Chem. Rev.* **2022**, *6*, 726–744.
[11] O. Habanjar, M. Diab-Assaf, F. Caldefie-Chezet, L. Delort, *Int. J. Mol. Sci.* **2021**, *22*, 12200.
[12] T. Saydé, O. El Hamoui, B. Alies, K. Gaudin, G. Lespes, S. Battu, *Nanomaterials* **2021**, *11*, 1–29.
[13] C. Li, A. G. Tebo, A. Gautier, *Int. J. Mol. Sci.* **2017**, *18*, 1473.
[14] J. B. Grimm, L. D. Lavis, *Nat. Methods* **2022**, *19*, 149–158.
[15] A. P. Demchenko, *Methods Appl. Fluoresc.* **2020**, *8*, 022001.
[16] L. C. C. Lee, K. K. W. Lo, *Chem. Rev.* **2024**, *124*, 8825–9014.
[17] R. Zhang, J. Yuan, *Acc. Chem. Res.* **2020**, *53*, 1316–1329.
[18] L. C. C. Lee, K. K. W. Lo, *J. Am. Chem. Soc.* **2022**, *144*, 14420–14440.
[19] C. Li, Y. Pang, Y. Xu, M. Lu, L. Tu, Q. Li, A. Sharma, Z. Guo, X. Li, Y. Sun, *Chem. Soc. Rev.* **2023**, *52*, 4392–4442.
[20] F. Monti, A. Baschieri, L. Sambri, N. Armaroli, *Acc. Chem. Res.* **2021**, *54*, 1492–1505.
[21] J. Zhou, J. Li, K. Y. Zhang, S. Liu, Q. Zhao, *Coord. Chem. Rev.* **2022**, *453*, 214334.
[22] Y. Yang, Y. Zhang, S. Xie, Y. Tang, Z. Zeng, B. Z. Tang, *Mater. Chem. Front.* **2021**, *5*, 3524–3548.
[23] S. Wei, Z. Li, W. Lu, H. Liu, J. Zhang, T. Chen, B. Z. Tang, *Angew. Chem. Int. Ed.* **2021**, *60*, 8608–8624.
[24] L. Liu, Z. Li, B. Yang, X. Jia, S. Wang, *Biomol. Eng.* **2024**, *14*, 620.
[25] T. T. C. Nguyen, C. K. Nguyen, T. H. Nguyen, N. Q. Tran, *Mater. Sci. Eng. C* **2017**, *70*, 992–999.
[26] I. S. Shin, J. Il Kim, T. H. Kwon, J. I. Hong, J. K. Lee, H. Kim, *J. Phys. Chem. C* **2007**, *111*, 2280–2286.
[27] M. Nonoyama, *Bull. Chem. Soc. Jpn.* **1974**, *47*, 767–768.
[28] E. Longhi, J. M. Fernandez-Hernandez, A. Iordache, R. Fröhlich, H. P. Josel, L. De Cola, *Inorg. Chem.* **2020**, *59*, 7435–7443.
[29] J. M. Fernandez-Hernandez, E. Longhi, R. Cysewski, F. Polo, H. P. Josel, L. De Cola, *Anal. Chem.* **2016**, *88*, 4174–4178.
[30] T. Y. Li, J. Wu, Z. G. Wu, Y. X. Zheng, J. L. Zuo, Y. Pan, *Coord. Chem. Rev.* **2018**, *374*, 55–92.
[31] J. Jayabharathi, V. Thanikachalam, S. Thilagavathy, *Coord. Chem. Rev.* **2023**, *483*, 215100.
[32] E. Knight, S. Przyborski, *J. Anat.* **2015**, *227*, 746–756.
[33] F. Fiorini, E. A. Prasetyanto, F. Taraballi, L. Pandolfi, F. Monroy, I. López-Montero, E. Tasciotti, L. De Cola, *Small* **2016**, *12*, 4881–4893.
[34] W. K. Subczynski, L. E. Hopwood, J. S. Hyde, *J. Gen. Physiol.* **1992**, *100*, 69–87.
[35] H. R. Jia, H. Y. Wang, Z. W. Yu, Z. Chen, F. G. Wu, *Bioconjugate Chem.* **2016**, *27*, 782–789.
[36] K. K. W. Lo, A. W. T. Choi, W. H. T. Law, *Dalton Trans.* **2012**, *41*, 6021–6047.
[37] R. Cao, J. Jia, X. Ma, M. Zhou, H. Fei, *J. Med. Chem.* **2013**, *56*, 3636–3644.
[38] C. Zhang, S. Jin, K. Yang, X. Xue, Z. Li, Y. Jiang, W. Q. Chen, L. Dai, G. Zou, X. J. Liang, *ACS Appl. Mater. Interfaces* **2014**, *6*, 8971–8975.
[39] R. Kreder, S. Oncul, O. A. Kucherak, K. A. Pyrshev, E. Real, Y. Mély, A. S. Klymchenko, *RSC Adv.* **2015**, *5*, 22899–22905.
[40] R. Kamitani, K. Niikura, T. Okajima, Y. Matsuo, K. Ijiro, *ChemBioChem* **2009**, *10*, 230–233.
[41] Y. Teramura, Y. Kaneda, T. Totani, H. Iwata, *Biomaterials* **2008**, *29*, 1345–1355.
[42] D. V. Krysko, T. Vanden Berghe, K. D'Herde, P. Vandenabeele, *Methods* **2008**, *44*, 205–221.
[43] B. J. Hoerl, R. E. Scott, *Virchows Arch. B Cell Path* **1978**, *27*, 335–345.
[44] K. K. W. Lo, P. K. Lee, J. S. Y. Lau, *Organometallics* **2008**, *27*, 2998–3006.
[45] K. Y. Zhang, K. K. W. Lo, *Inorg. Chem.* **2009**, *48*, 6011–6025.
[46] S. W. Youn, J. H. Bihn, *Tetrahedron Lett.* **2009**, *50*, 4598–4601.
[47] V. Fernández-Moreira, F. L. Thorp-Greenwood, A. J. Amoroso, J. Cable, J. B. Court, V. Gray, A. J. Hayes, R. L. Jenkins, B. M. Kariuki, D. Lloyd, C. O. Millet, C. F. Williams, M. P. Coogan, *Org. Biomol. Chem.* **2010**, *8*, 3888–3901.
[48] S. G. König, S. Öz, R. Krämer, *Mol. BioSyst.* **2016**, *12*, 1114–1117.
[49] S. Bakthavatsalam, A. Sarkar, A. Rakshit, S. Jain, A. Kumar, A. Datta, *Chem. Commun.* **2015**, *51*, 2605–2608.
[50] C. A. Puckett, J. K. Barton, *J. Am. Chem. Soc.* **2007**, *129*, 46–47.
[51] K. K. W. Lo, K. K. S. Tso, *Inorg. Chem. Front.* **2015**, *2*, 510–524.
[52] E. Reaven, L. Tsai, S. Azhar, *J. Biol. Chem.* **1996**, *271*, 16208–16217.

Manuscript received: January 3, 2025
Accepted manuscript online: January 19, 2025
Version of record online: March 6, 2025